Research Article

INVESTIGATION OF TRANSIENTS IN GROUNDING GRIDS

Basma M. SAMY[1], *Ibrahim I. I. MANSY*[2], *Ebrahim A. BADRAN*[2,3,*]

[1]Higher Institute of Engineering and Technology in El-Mahalla, El-Mahala El-kubra, Egypt
[2]Electrical Engineering Department, Mansoura university, Mansoura, Egypt
[3]Mansoura Higher Institute of Engineering and Technology (Mansoura Collage), El-Mansoura, Egypt

basbosasamy2012@gmail.com, mansy@mans.edu.eg, ebadran@mans.edu.eg

[*]Corresponding author: Ebrahim A. Badran; ebadran@mans.edu.eg

DOI: 10.15598/aeee.v22i4.240412

Article history: Received Apr 26, 2024; Revised Sep 08, 2024; Accepted Oct 08, 2024; Published Dec 31, 2024.

Abstract. *The grounding grid of a power system is very important for absorbing the harmful overvoltages and/or overcurrents during transients. The lightning surges frequently causes overvoltages and/or overcurrents via the grounding grid. This may have dangerous effects on persons and/or equipment. Therefore, this paper reviews in detail the transient in grounding grids due to lightning surges. The grounding grid configurations and mathematical modeling are explained. Many configurations are used in the analysis such as one, four, sixteen meshes grounding configurations. Also, two injection points are analyzed: at the terminal and the middle of the grid. The analysis is carried out using ATP/EMTP. Many transient responses of voltages and currents at different points of the grounding grid for different configurations are calculated and compared. The peak voltage and current values are compared to be the basis of safety design of the grounding system.*

Keywords

Lightning, Overvoltage, Overcurrent, Mitigation, Grounding Grids, ATP/EMTP.

1. Introduction

The framework of power systems is structured around specific points like generator and transformer neutral points [1]. Grounding grids play a key role in reducing overvoltage during short-circuit events. These grids consist of conductive segments acting as grounding units.

Grounding systems in substations are essential for safety and reliability, aiming to maintain touch and step voltages within established standards [2]. A grounding grid includes interconnected horizontal conductors and rods, with the primary goal of meeting safety levels set by industry standards [3]. Various grounding methods are studied to enhance human safety around grounding grids and electrical equipment [4].

Improving grounding grid performance involves addressing two key areas: reducing fault current and refining grid design [5]. Decreasing fault current is challenging [6] but can be achieved by adjusting the grid's mesh and adding vertical grounding rods [7, 8], enhancing protection against electric shocks [9].

Grounding systems have multiple functions, such as neutral grounding of transformers, dissipating overhead ground overvoltage, balancing charge between phases and ground, and providing equipment grounding [10]. Proper grounding is crucial for defense against lightning, ensuring operator and equipment safety [11]. Inadequate grounding can lead to damage, data and equipment loss, plant shutdowns, and safety risks [12]. Electric power companies are working to improve grounding systems for safety and reliability [13].

Grounding system performance is affected by factors such as grounding current, so monitoring and assessing grounding conditions is an ongoing area of research [14]. Due to the difficulty of observ-

ing overvoltage directly, numerical simulations like the Alternative/ElectroMagnetic Transient Program (ATP/EMTP) are used for investigation [15].

In this paper, a detailed overview and brief discussion of grounding grids are introduced. The grounding grid configurations and mathematical modeling are explained. Many configurations are used in the analysis such as one, four, sixteen meshes grounding configurations. Also, two injection points are analyzed: at the terminal and the middle of the grid. The analysis is carried out using ATPDraw version of ATP/EMTP [16]. Many transient responses of voltages and currents at different points of the grounding grid for different configurations are calculated and compared. The peak voltage and current values are compared to be the basis of safety design of the grounding system.

The subsequent sections of the paper are organized as follows: Section 2. covers grounding configuration and modeling, Section 3. delves into the transient behavior of grounding grids, Section 4. presents simulations of several illustrative cases, and finally, Section 5. summarizes the conclusions.

2. Grounding Grid Configuration And Modeling

Various methods have been used over the years to analyze and optimize grounding grid design and configuration [17]. Uneven spacing of grid elements has demonstrated improved performance in some cases, with factors like fault current, soil resistivity, and conductor length contributing to lower and more evenly distributed touch voltages [18].

An experimental approach is presented in one study [19], while another introduced the concept of a "Compression ratio" conductor [20, 21]. Other techniques based on genetic algorithms are applied in different studies [22, 23]. An evolutionary approach is often preferred as it optimizes the grounding grid's layout without relying on fixed structures or previous experience.

The grounding grid is composed of bars positioned at a specific depth beneath the substation floor, spanning the entire substation area. Grounding rods are strategically placed within the mesh, extending downward to areas like building and transformer foundations [24].

Fig. 1a provides a detailed view of the grounding grid components [25], while Fig. 1b illustrates the grounding electrodes, including inductances and resistances. The resistance (R) and self-inductance (L) are

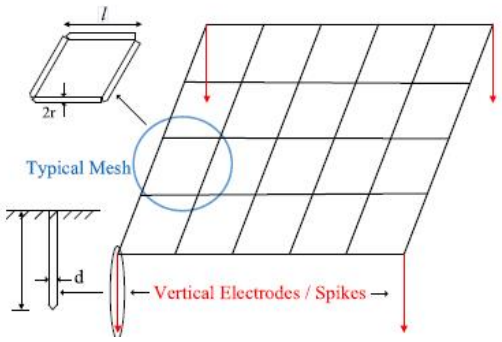

(a) The three-dimensional view.

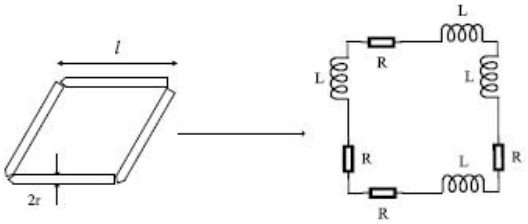

(b) Parameters of the grounding electrodes model.

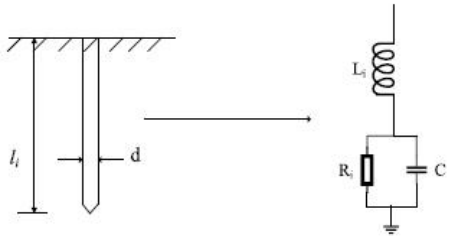

(c) The equivalent circuit for vertical rod/spike.

Fig. 1: Equivalent circuit of the ground Grid.

determined using equations (1) and (2).

$$R = \frac{\rho}{\pi r^2} [\Omega] \tag{1}$$

$$L = \frac{\mu_o l}{2\pi} \left[\ln \left(\frac{2l}{\sqrt{2rh}} \right) - 1 \right] [\mathrm{H}] \tag{2}$$

where l is the length of each cell, r is the electrode radius, ρ_{cu} is the material resistivity, h is the depth and the permeability is assumed as the vacuum permeability, $\mu_0 = 4\pi 10^{-7}$ A/m [26]. Also, the grounding resistance, R_t and the capacitance to ground are determined by:

$$R_t = \frac{\rho}{\pi l} \left[\ln \left(\frac{2l}{\sqrt{2rh}} \right) - 1 \right] [\Omega] \tag{3}$$

$$C = \frac{\pi \varepsilon l}{\ln \left(\frac{2l}{\sqrt{2rh}} \right) - 1} [F] \tag{4}$$

In this context, the resistivity of the soil (ρ) is a key parameter, and it's important to note that the

permittivity (ε) is defined as $\varepsilon = \varepsilon_0 \varepsilon_r$, where $\varepsilon_0 = 8.859 \times 10^{-12}$ F/m represents the vacuum permittivity, and ε_r denotes the relative permittivity of the soil [26].

The equivalent circuit of the vertical rod/spike is shown in Fig. 1c. The resistance, inductance, and capacitance under transient phenomenon are calculated by:

$$R_i = \frac{\rho}{l_i}\left(\ln\frac{8l_i}{d} - 1\right)[\Omega] \tag{5}$$

$$L_i = 2l_i\left(\ln\frac{4l_i}{d} \times 10^{-7}\right)[\mathrm{H}] \tag{6}$$

$$C = \frac{\varepsilon_r l_i}{18\ln\left(\frac{4l_i}{d}\right)} \times 10^{-9}\,[F] \tag{7}$$

where, ρ is solid resistivity (Ωm), l_i is the total length of ground rod (m), d is the diameter of the ground rod (m), and ε_r is the relative permittivity of solid.

3. Grounding Grid Behavior Via Transients-Litrature Review

The industrial sector requires a reliable and cost-effective way to monitor the safety of grounding grids to protect people and equipment. A monitoring system for assessing substation safety was created in [27], incorporating telecom and sensor technology as part of the smart grid initiative. It uses a set frequency to periodically measure touch and step voltages and relies on a database for efficient grounding grid evaluation.

For better equipment protection, the plan should expand to include additional sensors and indices. The grounding design also focuses on protecting equipment, with a hypothesis suggesting that appropriate touch and step voltages in various substation locations indicate good grounding conditions for equipment protection. However, further research is needed to confirm this hypothesis. The plan involves a sensor network and data collection, which poses challenges such as network creation, maintenance, and reliability, aligning with the goals of smart grid researchers focused on information and communication technology (ICT).

In terms of grounding grid design, the main aim is to reduce grounding resistance, mesh voltage, and step voltage to acceptable levels during a ground fault. It's also essential to evaluate the grid's performance after a lightning strike, as it behaves differently under impulse current compared to power-frequency failures. The ATP-EMTP software assesses the grounding grid's effectiveness during lightning strikes. Various methods to decrease induced and lightning overvoltage involve modifying the grid design by adding conductors or rods to increase the grid's surface area in contact with the soil.

One approach, the IEEE method, involved placing a single rod of different lengths at the point of the lightning wave's impact. An optimal rod length of 3 meters has been found, as longer lengths increase induced overvoltage due to frequency-dependent inductive effects [28].

An external ground design in distribution systems aimed to improve lightning performance by connecting an external ground wire and ground rod to overhead wires [29]. An ATP-EMTP model simulates lightning performance, including pole top voltage, critical current, and back flashover rate (BFOR), using different impulse resistances and lightning current waveforms. Installing an external ground affects pole top voltage, critical current, and BFOR, depending on factors such as lightning current waveform, wave velocity, and ground rod impulse resistance. These findings guide transmission line grounding system designs and grounding standards revisions.

Another study introduced a transient methodology for calculating node voltages and uses a genetic algorithm to optimize grounding grid size for studying the effects of lightning strikes [24]. Simulation results with varying mesh grid sizes provide insights into the behavior and impedance of the grounding system during lightning strikes. The study examines ground potential rise (GPR) and mesh grid size to enhance safety, finding that irregular grounding grids tend to be more secure, with lower total GPR compared to regular grids.

Another investigation examined the transient behavior of grounding systems under lightning strikes using circuit models [26]. These models include current-controlled voltage sources (CCVS) to represent interactions among grounding electrodes and simulate complex grounding grids under surge conditions. The models align with EMF theory models despite approximations related to circuit representations during surge conditions. Further research is suggested to improve performance at lower frequencies and examine the model's potential for simulating complex grounding arrangements.

While circuit models are limited by low-frequency quasi-static approximations, EMF theory models offer more accuracy but struggle with complex geometries. Field theory-based models often overlook ionization effects. The circuit approach can be extended to higher frequencies by dividing the electrode representation into basic cells, but it may overestimate transient voltages due to quasi-static assumptions [30].

Lastly, a case study at the Al-Mostakbal substation in Cairo, Egypt, evaluated grounding grid design under different conditions, including ground faults and lightning strikes [28]. The study highlights the importance of assessing grounding grid performance during lightning strikes, where impulse currents cause different behavior than power-frequency failures.

Various strategies are examined to mitigate induced overvoltage, focusing primarily on changing grid design to increase contact surface with the soil. The IEEE method recommends using a 3-meter rod at the point of lightning impact to reduce induced overvoltage. ATP-EMTP simulations assess the effectiveness of these methods.

Moreover, a study explores grounding system modeling for ground potential rise (GPR) computation, power system simulations, and insulation coordination [31]. It proposed a method to predict equivalent circuit parameters through time-domain impulse response optimization. Equivalent circuits that accurately represent grounding systems while accounting for frequency effects and soil ionization are developed. Nonlinear circuits improve response accuracy, reducing errors in GPR estimation to less than 4%. These circuits apply to systemic analyses and GPR calculations considering lightning strikes and short circuits.

While many electromagnetic transient (EMT) investigations focus on overvoltage behavior across a wide frequency range, overcurrent of grounding grid's effects receives less attention.

4. Grounding Grid Simulation and Analysis

4.1. Grounding Grid Simulation

To examine the transient response of grounding grids accurately, it is crucial to conduct simulations of these grids. In this research, the transient response to lightning impulses using various tested grids: CS01, CS04, and CS16, as depicted in Fig. 2 are analyzed for many cases. The dimensions of these test cases are detailed in Table 1. The horizontal grounding grid conductors have a radius of 10 mm and are buried at a depth of 0.6 m in soil with $\varepsilon = 50$ and $\rho = 100\Omega$m [32]. The current impulse injected at point A in each grid follows the formula presented in equation (8). The peak value of this current impulse is approximately 12 kA. The peak current and the time constants are selected as given in [32] for comparison purpose.

$$I(t) = 12000\left(e^{-27000t} - e^{-5600000t}\right) \tag{8}$$

The first point of injection is point A at the terminal of the grid, whereas the second point is point B at the middle of the grid, as given in Fig. 2 Fig. 3 illustrates the ATPDraw model employed for these test cases. Table 2 provides the RLC parameters for the grids under investigation, where R and C represent the resistance and capacitance of the grid, while L1 and L2 denote the inductance of the main wire and the grid conductors.

Fig. 4 presents the comparison between the published in [32] and simulated voltage waveform at the outlet point for both one and four meshes grounding grid as response to the lightning impulse at point A. It can be seen the closeness between the waveforms and hence the availability of the proposed model using ATPDraw.

Tab. 1: RLC for each grid configuration.

	$R\,(\Omega)$	$L1(H)$	$C(F)$	$L2(H)$
CS01	6.499	2.396e-005	6.802e-09	5.529e-006
CS04	5.665	2.396e-005	7.803e-09	5.529e-006
CS16	1.071	1.412e-004	4.125e-08	3.301e-005

4.2. Analysis of Grounding Grid's Voltages

The analysis of grounding grid's voltage is carried out via the investigation of the grid response when the injection is applied at two points; terminal point A and middle point B.

1) Injection at the terminal point A

The lightning impulse is applied in this case at point A. The waveforms of the transient voltages in response to a lightning impulse for different grounding grid configurations are illustrated. In Fig. 5, the voltage waveforms at the outlet point for one, four, and sixteen grounding grid meshes are observed.

Also, Fig. 6 shows the transient voltage waveforms at points B2 and B3 at one mesh configuration and the same point at various grid configurations in response to the lightning impulse. Additionally, Fig. 7 displays the transient voltage waveforms at several points for each grid configuration in response to the same lightning impulse.

The above analysis is carried out again when the three terminals of the ground grid are earthed via the vertical rod. Fig. 8 illustrates the transient voltage waveforms at the three terminals of both one and four meshes' ground grid configurations. Furthermore, Fig. 9 shows the comparison between the voltage of the same terminal point for the three ground grid configurations under study.

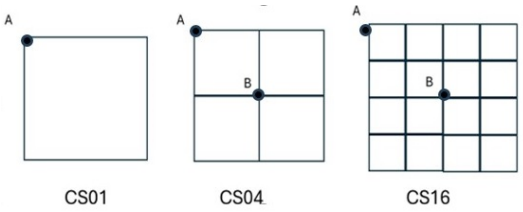

Fig. 2: Different number of meshes for square grids.

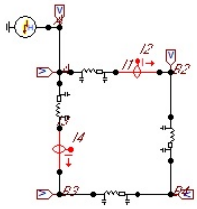

(a) CS01.

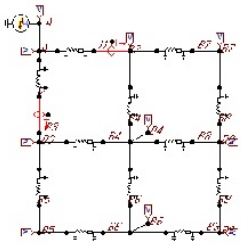

(b) CS04.

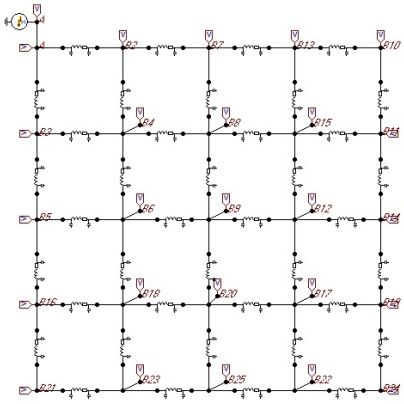

(c) CS16.

Fig. 3: ATPDraw simulation models for different cases.

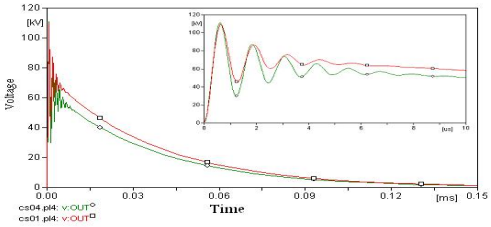

(a) Published.

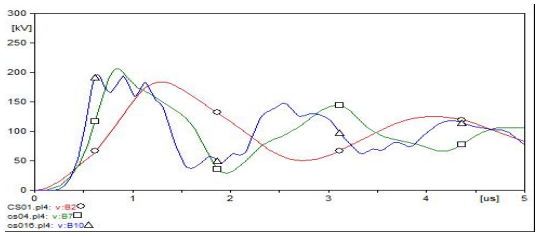

(a) B2 at one mesh.

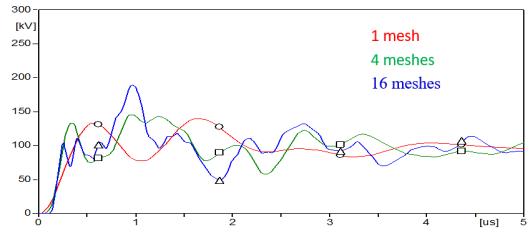

(b) B3 at one mesh.

Fig. 6: The voltage waveforms at terminal points for different grids as response to the lightning impulse at point A without earthing the terminals.

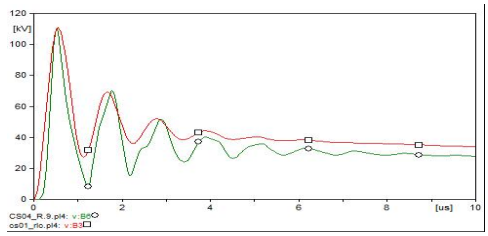

(b) Simulated.

Fig. 4: Comparison between the published and simulated voltage waveform at the outlet point for both 1 and 4 meshes as response to the lightning impulse.

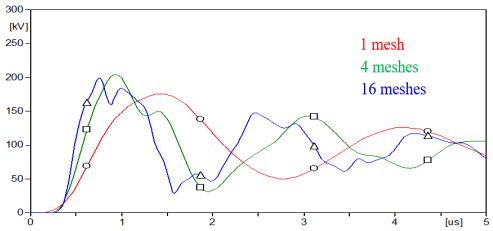

Fig. 5: The voltage waveform at the outlet point for 1, 4, and 16 meshes as response to the lightning impulse at point A.

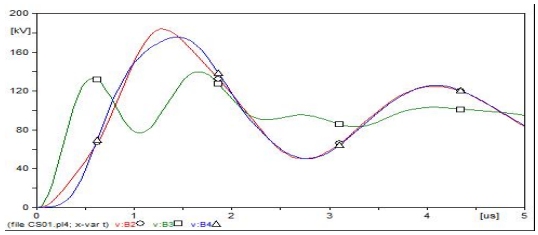

(a) 1 mesh.

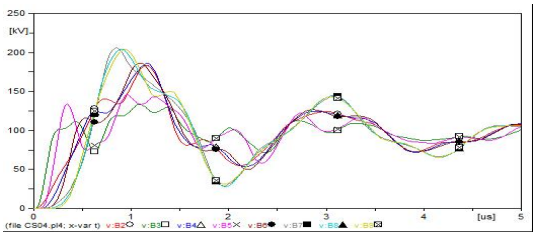

(b) 4 meshes.

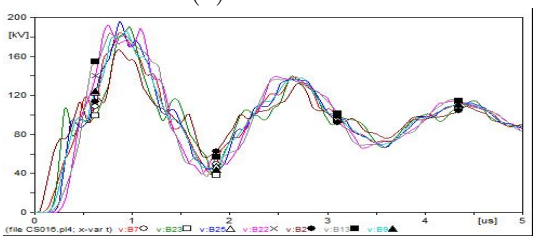

(c1) 16 meshes.

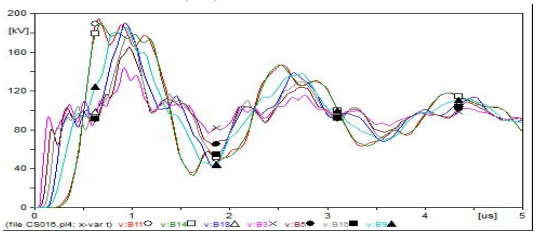

(c2) 16 meshes.

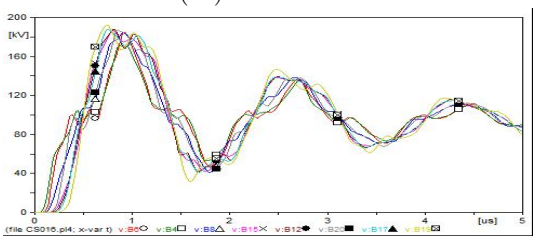

(c3) 16 meshes.

Fig. 7: The voltage waveforms at several points for different grid configurations as response to the lightning impulse at point A without earthing the terminals.

Fig. 10 shows the comparison between the transient voltage waveforms at many points of the four meshes configurations when the three terminals are earthed. Also, Fig. 11 shows the comparison between the transient voltage waveforms at many points of the sexteen meshes configurations when the three terminals are earthed.

It can be seen that nonlinearity of voltages waveform and the peaks. Also, the earthing of the main terminals reduces the peak values.

2) Injection at the terminal point B

Again for more investigation of the response of the grounding grid to the lightning impulse, the injection of the lightning is applied in this case at point B. The waveforms of the transient voltages in response to a lightning impulse for different grounding grid configurations are illustrated.

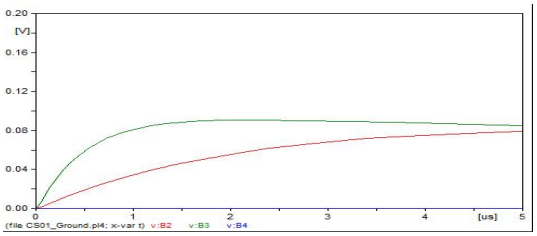

(a) 1 mesh.

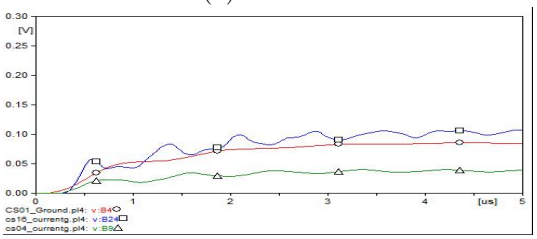

(b) 4 meshes.

Fig. 8: The voltage waveform at the three terminal points for 1 and 4 meshes as response to the lightning impulse at point A with earthing of the three terminals.

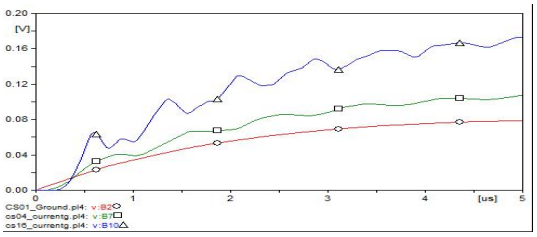

(a) B2.

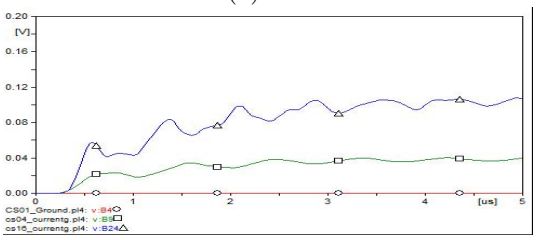

(b) B4.

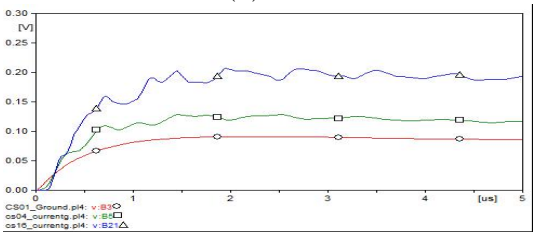

(c) B3.

Fig. 9: The voltage waveforms at terminal points of the one mesh and their equivalents for different grids as response to the lightning impulse at point A with earthing of the three terminals.

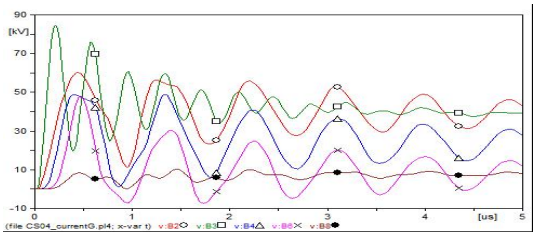

Fig. 10: The voltage waveforms at several points of the four grid configuration as response to the lightning impulse at point A with earthing of the three terminals.

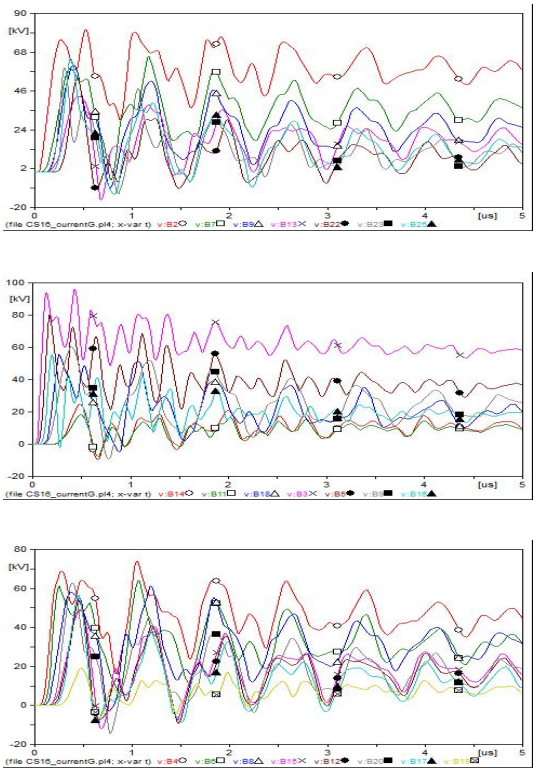

Fig. 11: The voltage waveforms at several points of the sexteen grid configuration as response to the lightning impulse at point A with earthing of the three terminals.

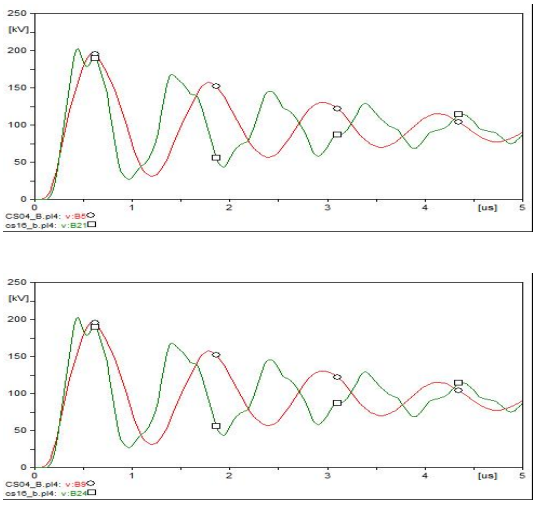

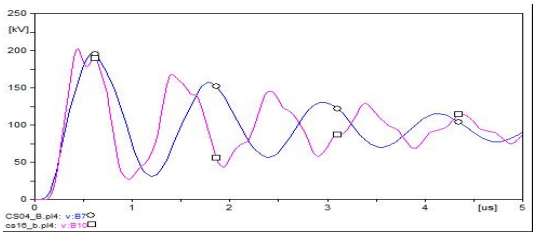

Fig. 12: The voltage waveforms at the terminal points for different grids as response to the lightning impulse at point B without earthing of the terminals.

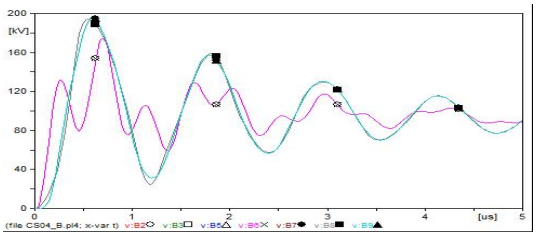

Fig. 13: The voltage waveforms at several points for the four meshes' grid as response to the lightning impulse at point B without earthing of the terminals.

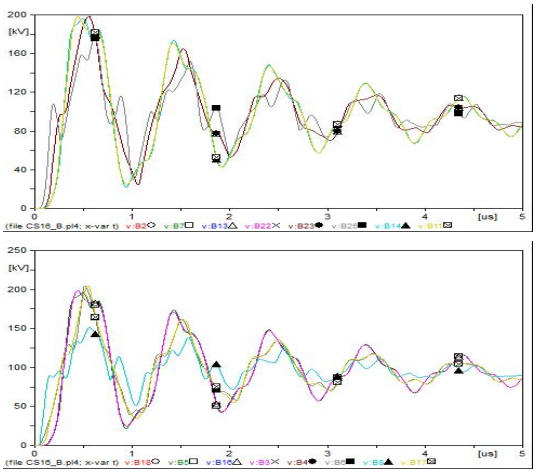

Fig. 14: The voltage waveforms at several points for the sexiteen meshes' grid as response to the lightning impulse at point B without earthing of the terminals.

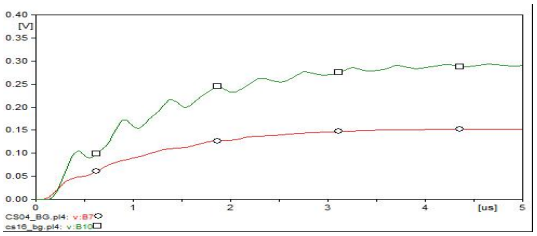

Fig. 15: The voltage waveforms at the terminal points for different grids as response to the lightning impulse at point B with earthing of the terminals.

Fig. 12 shows the transient voltage waveforms at the teminal points for various grid configurations in response to the lightning impulse at point B. Additionally, Figs. 13 and 14 display the transient voltage waveforms at several points for each of four and sexiteen grid configuration in response to the same lightning impulse.

The above analysis is carried out again when the three terminals of the fround grid are earthed via the vertical rod. Fig. 15 illustrates the transient voltage waveforms at the three terminals of both one and four meshes' ground grid configurations. Furthermore, Fig. 16 shows the comparison between the voltage of the same terminal point for the three ground grid confiurations under study.

4.3. Analysis of Grounding Grid's Currents

The analysis of grounding grid's currents is carried out via the investigation of the grid response when the injection is applied at two points; terminal point A and the middle point B. Also, the terminals of the main sides are not grounded and then grounded as two case studies as given before.

1) Injection at the terminal point A

The injection of the lightning impulse is applied in this case at point A. The waveforms of the transient currents in response to a lightning impulse for different grounding grid configurations are illustrated.

The terminals of the main sides are not grounded

Fig. 17a shows the currents of the four branches of the one mesh grounding grid configuration (CS01).

Fig. 17b shows the currents of the branches of the first mesh of four meshs grounding grid configuration (CS04). Also, Fig. 17c shows the currents of the branches of the first mesh of sexiteen meshs grounding grid configuration (CS16).

The currents of the two branches connected to the injection point are increased with the increasing of the grounding grid meshes. It is increased for the one, four, sixteen meshes as 1598 A, 3954 A, and 6766A, respectively. Therefore, it can be concluded that the ground grid currents at the first mesh are increased as the number of meshes increased.

Fig. 18 illustrates the distribution of currents in several pathes of the four meshes configuration for the right path (I1, I7, I21, and I17), the left path (I3, I9, I11, and I15), and the two middle pathes; middle path1 (I1, I23, I13, and I15) and middle path 2 (I3, I5, I19, and I17).

It can be notice that the oscillatory behaviour of the current increases at the end of each path where the current go to the earth.

Fig. 19 illustrates the distribution of currents in several pathes of the sixteen meshes configuration illustrates the right path (I1, I2, I4, I6, I23, I24, I59, I77), the middle right path (I1, I2, I4, I19, I27, I55, I73, I74), the middle path (I1, I2, I15, I29, I51, I67, I70, I74), the middle left path (I1, I11, I31, I37, I38, I55, I73, and I74), the left path (I9, I32, I43, I61, I62, I68, I70, and I74), the left-middle path (I9, I32, I43, I48, I52, I56, I77).

It can be noticed that the oscillatory behaviour of the current increases at the end of each path where the current goes to the earth.

The terminals of the main sides are grounded

Fig. 20a shows the currents of the four branches of the one mesh grounding grid configuration (CS01). Fig. 20b shows the currents of the branches of the first mesh of four meshes grounding grid configuration (CS04). Also, Fig. 20c shows the currents of the branches of the first mesh of sixteen meshes grounding grid configuration (CS16).

The currents of the two branches connected to the injection point are increased with the increasing of the grounding grid meshes. It is increased for the one, four, sixteen meshes as 9059 A, 13857 A, and 24448 A, respectively. Therefore, it can be concluded that the ground grid currents at the first mesh are increased as the number of meshes increased.

Fig. 21 illustrates the distribution of currents in several pathes of the four meshes configuration for the right path (I1, I7, I21, and I17), the left path (I3, I9, I11, and I15), and the two middle pathes; middle path1 (I1, I23, I13, and I15) and middle path 2 (I3, I5, I19, and I17).

It can be notice that the oscillatory behaviour of the current increases at the end of each path where the current go to the earth.

Fig. 22 illustrates the distribution of currents in several pathes of the sixteen meshes configuration illustrates the right path (I1, I2, I4, I6, I23, I24, I59, I77), the middle right path (I1, I2, I4, I19, I27, I55, I73, I74), the middle path (I1, I2, I15, I29, I51, I67, I70, I74), the middle left path (I1, I11, I31, I37, I38, I55, I73, and I74), the left path (I9, I32, I43, I61, I62, I68, I70, and I74), the left-middle path (I9, I32, I43, I48, I52, I56, I77).

It can be noticed that the oscillatory behaviour of the current increases at the end of each path where the current goes to the earth.

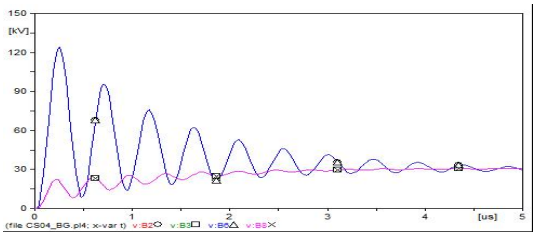

(a) Four meshes' grid.

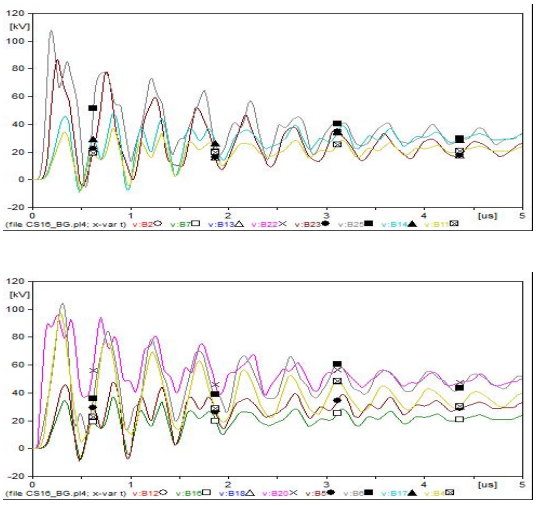

(b) Sexteen meshes' grid.

Fig. 16: The voltage waveforms at several points for the meshes' grid as response to the lightning impulse at point B with earthing of the terminals.

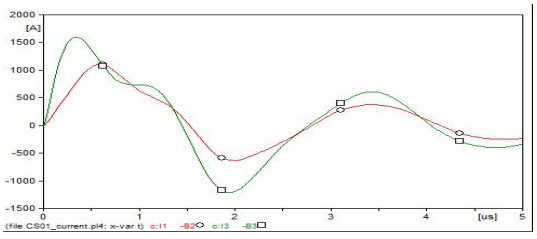

(a) 1 mesh.

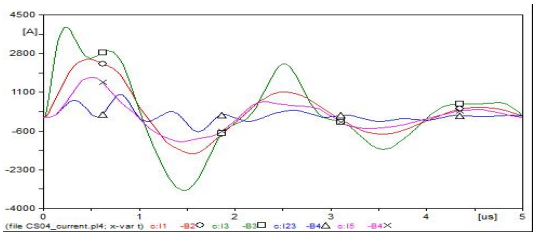

(b) 4 meshes.

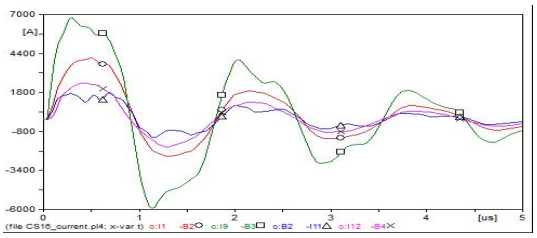

(c) 16 meshes.

Fig. 17: Currents of all branches of the first mesh of different grid configurations as response to the lightning impulse at point A.

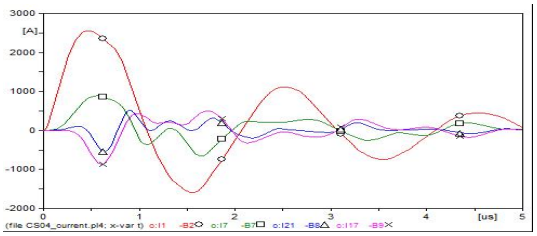

(a) The right path.

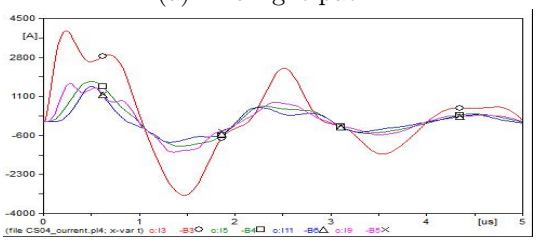

(b) The left path.

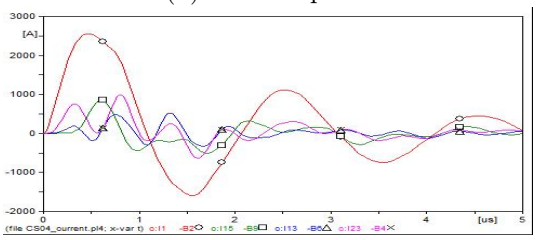

(c) The middle path 1.

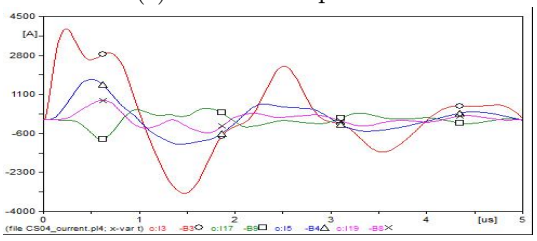

(d) The middle path 2.

Fig. 18: Currents of all branches of four meshes grid as response to the lightning impulse at point A.

A. Injection at the terminal point B

Again for more investigation of the response of the grounding grid to the lightning impulse, the injection of the lightning is applied in this case at point B. The waveforms of the transient currents in response to a lightning impulse for different grounding grid configu-

rations are illustrated. The terminals of the main sides are not grounded and then grounded as two case studies.

The terminals of the main sides are not grounded

Fig. 23a shows the currents of the branches of the first mesh of four meshs grounding grid configuration (CS04). Also, Fig. 23b shows the currents of the branches of the first mesh of sexiteen meshs grounding grid configuration (CS16).

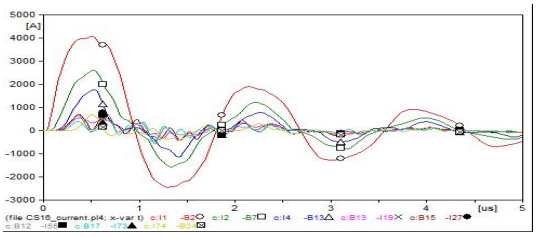

(a) The right path.

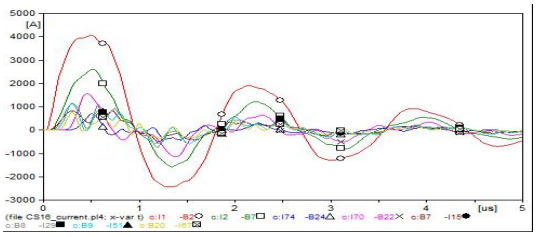

(b) The middle-right path.

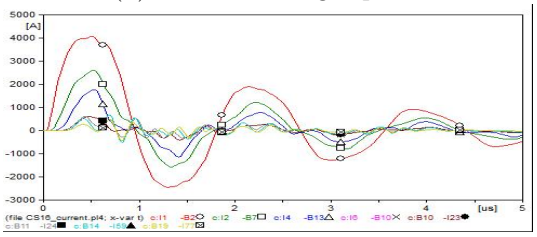

(c) The middle path.

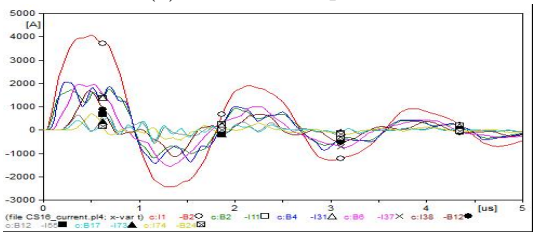

(d) The middle-left path.

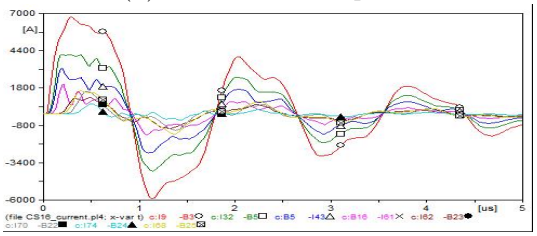

(e) The left path.

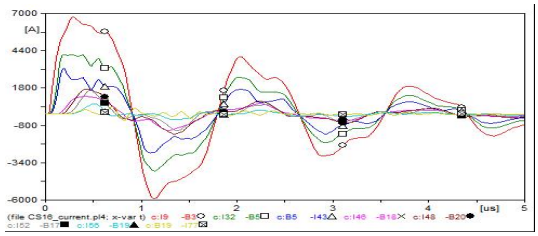

(f) The left-middle path.

Fig. 19: Currents of all branches of four meshes grid as response to the lightning impulse at point A.

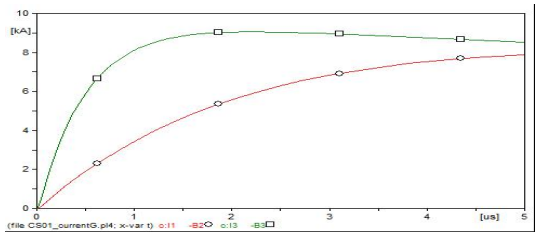

(a) 1 mesh.

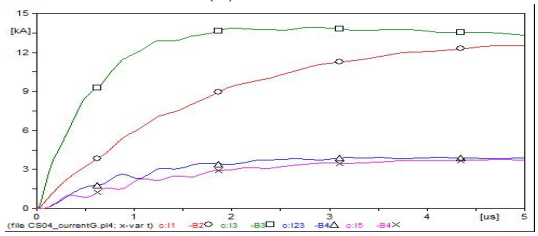

(b) 4 meshes.

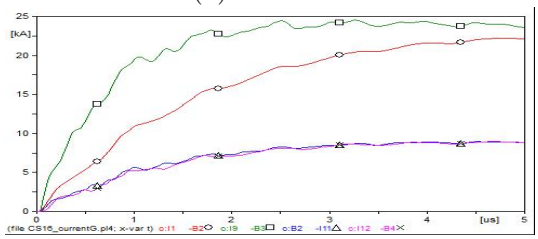

(c) 16 meshes.

Fig. 20: Currents of all branches of the first mesh of different grid configurations as response to the lightning impulse at point A.

Fig. 24 illustrates the distribution of currents in several pathes of the four meshes configuration for the right path (I1, I7, I21, and I17), the left path (I3, I9, I11, and I15), and the two middle pathes; middle path1 (I1, I23, I13, and I15) and middle path 2 (I3, I5, I19, and I17).

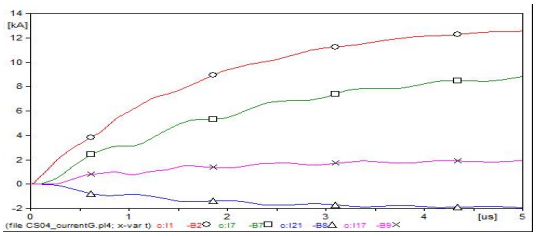

(a) The right path.

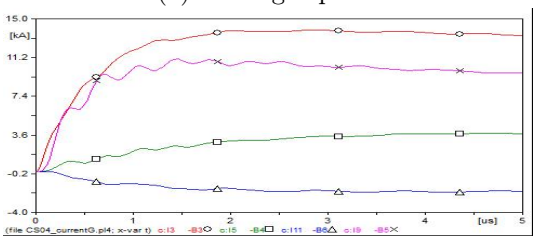

(b) The left path.

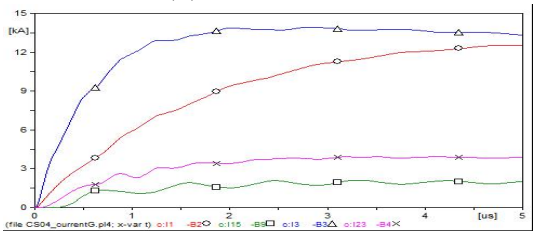

(c) The middle path 1.

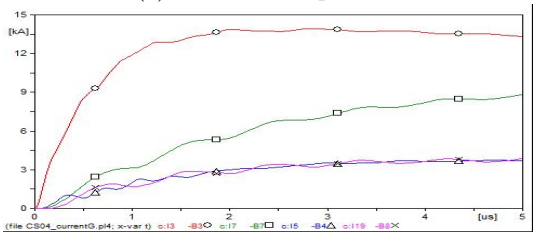

(d) The middle path 2.

Fig. 21: Currents of all branches of four meshes grid as response to the lightning impulse at point A.

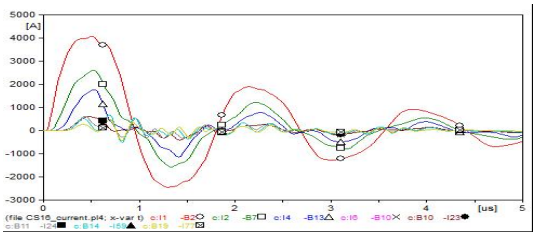

(c) The middle path.

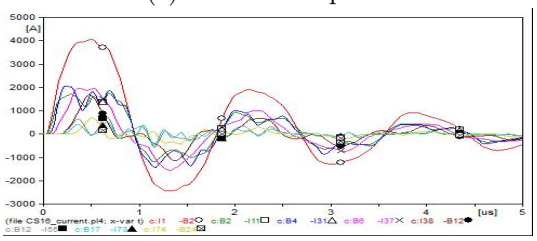

(d) The middle-left path.

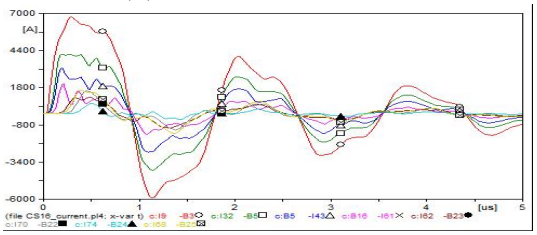

(e) The left path.

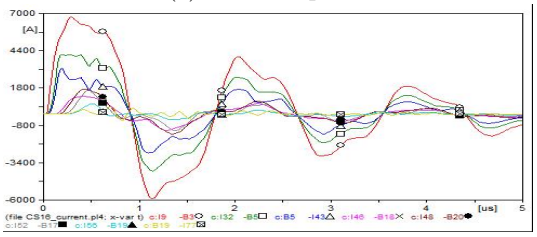

(f) The left-middle path.

Fig. 22: Currents of all branches of sixteen meshes grid as response to the the lightning impulse at point A.

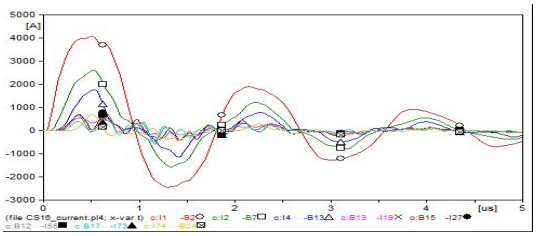

(a) The right path.

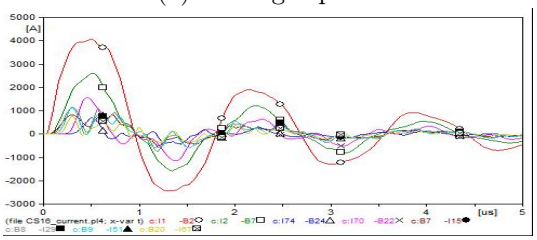

(b) The middle-right path.

It can be notice that the oscillatory behaviour of the current increases at the end of each path where the current go to the earth.

Fig. 25 illustrates the distribution of currents in several pathes of the sixteen meshes configuration illustrates the right path (I1, I2, I4, I6, I23, I24, I59, I77), the middle right path (I1, I2, I4, I19, I27, I55, I73, I74), the middle path (I1, I2, I15, I29, I51, I67, I70, I74), the middle left path (I1, I11, I31, I37, I38, I55, I73, and I74), the left path (I9, I32, I43, I61, I62, I68, I70, and I74), the left-middle path (I9, I32, I43, I48, I52, I56, I77).

The terminals of the main sides are grounded

Fig. 26a shows the currents of the branches of the first mesh of four meshs grounding grid configuration (CS04). Also, Fig. 26b shows the currents of the branches of the first mesh of sexiteen meshs grounding grid configuration (CS16).

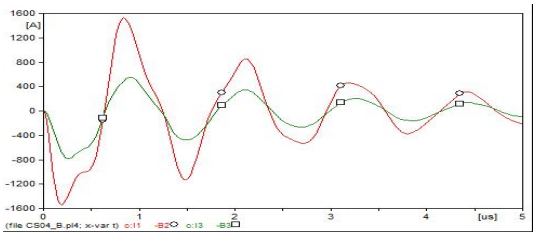

(a) 4 meshes.

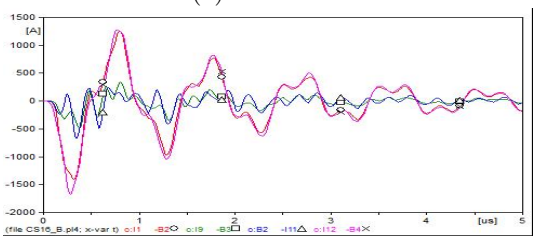

(b) 16 meshes.

Fig. 23: Currents of all branches of the first mesh of different grid configurations as response to the lightning impulse at point B.

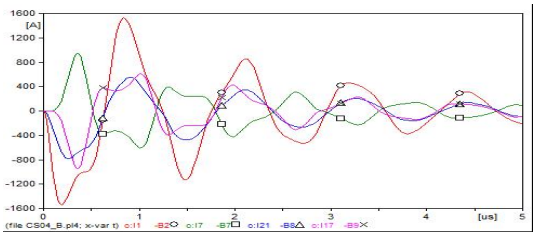

(a) The right path.

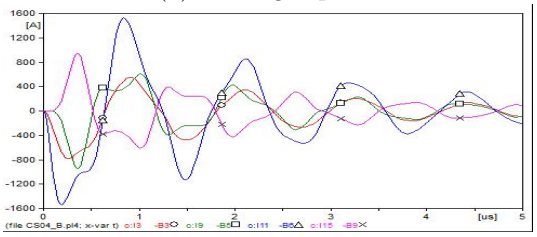

(b) The left path.

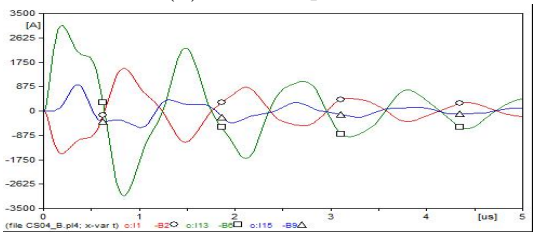

(c) The middle path 1.

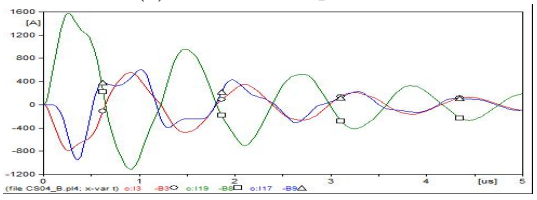

(d) The middle path 2.

Fig. 24: Currents of all branches of four meshes grid as response to the lightning current impulse at point B.

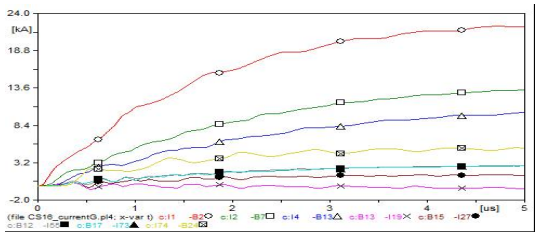

(a) The right path.

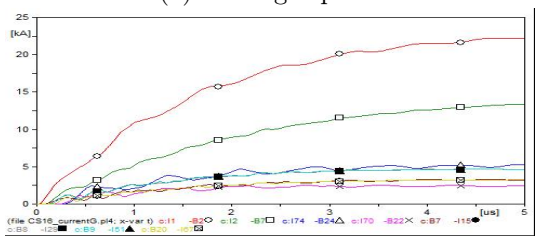

(b) The middle-right path.

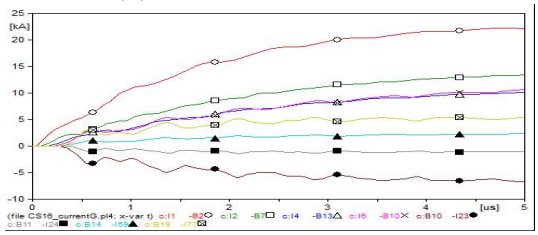

(c) The middle path.

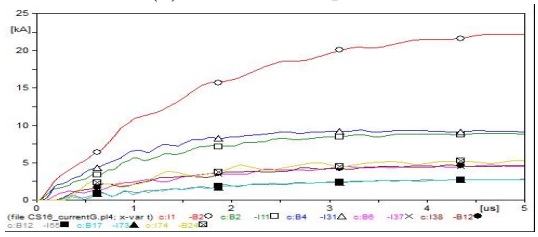

(d) The middle-left path.

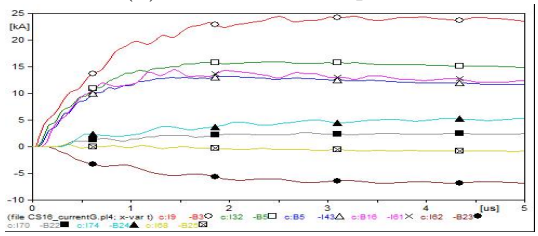

(e) The left path.

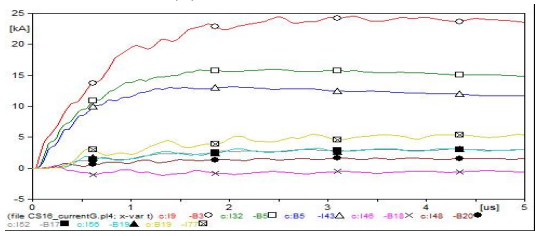

(f) The left-middle path.

Fig. 25: Currents of all branches of sixteen meshes grid as response to the lightning current impulse at point B.

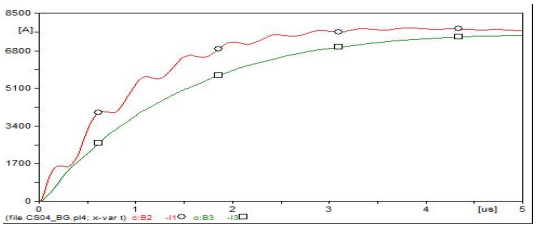

(a) 4 meshes.

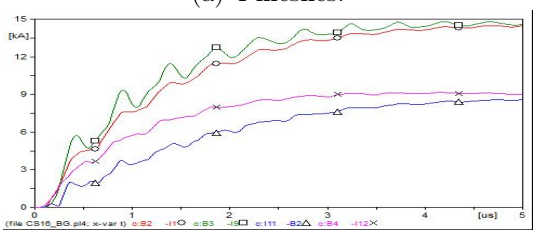

(b) 16 meshes.

Fig. 26: Currents of all branches of the first mesh of different grid configurations as response to the lightning impulse at point B.

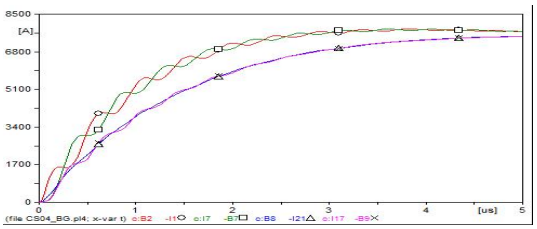

(a) The right path.

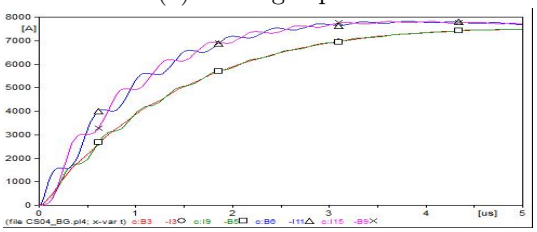

(b) The left path.

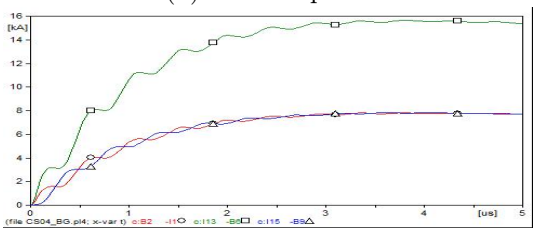

(c) The middle path 1.

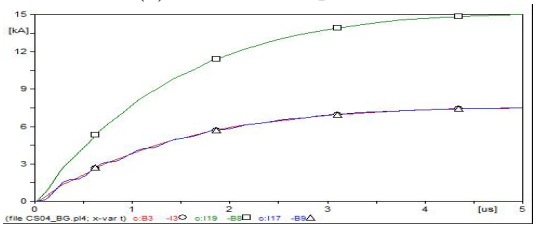

(d) The middle path 2.

Fig. 27: Currents of all branches of four meshes grid as response to the lightning current impulse at point B.

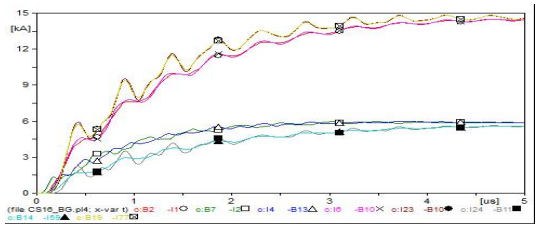

(a) The right path.

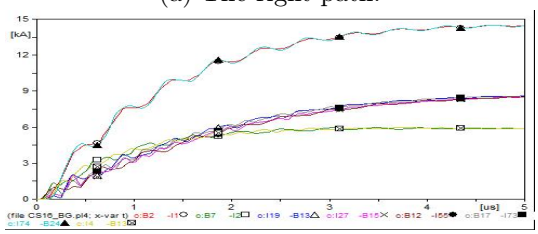

(b) The middle-right path.

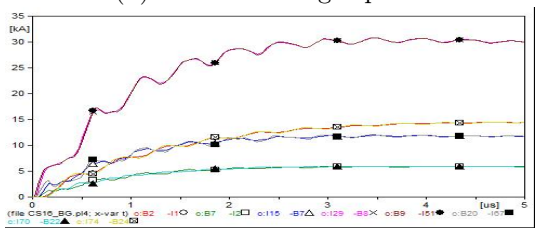

(c) The middle path.

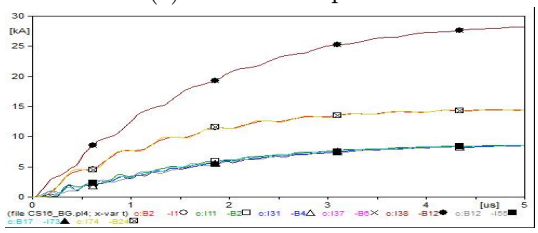

(d) The middle-left path.

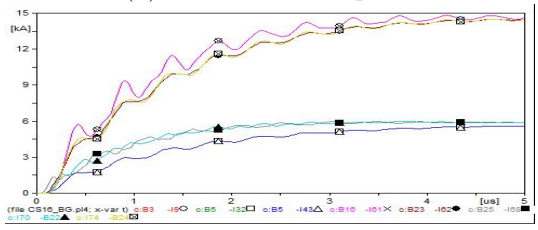

(e) The left path.

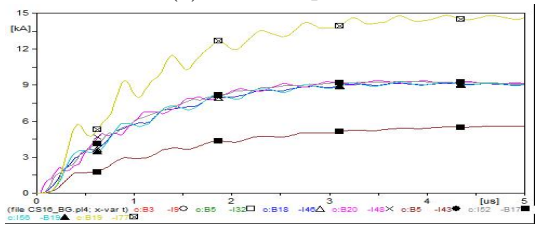

(f) The left-middle path.

Fig. 28: Currents of all branches of sixteen meshes grid as response to the lightning current impulse at point B.

Fig. 27 illustrates the distribution of currents in several pathes of the four meshes configuration for the right path (I1, I7, I21, and I17), the left path (I3, I9, I11, and I15), and the two middle pathes; middle path1

(I1, I23, I13, and I15) and middle path 2 (I3, I5, I19, and I17).

Fig. 28 illustrates the distribution of currents in several pathes of the sixteen meshes configuration illustrates the right path (I1, I2, I4, I6, I23, I24, I59, I77), the middle right path (I1, I2, I4, I19, I27, I55, I73, I74), the middle path (I1, I2, I15, I29, I51, I67, I70, I74), the middle left path (I1, I11, I31, I37, I38, I55, I73, and I74), the left path (I9, I32, I43, I61, I62, I68, I70, and I74), the left-middle path (I9, I32, I43, I48, I52, I56, I77).

It can be notice that the oscillatory behaviour of the current increases at the end of each path where the current go to the earth.

5. Conclusion

In this paper, the transient in the grounding grid due to lightning surges is discussed. the grounding grid configurations and mathematical modeling are explained. Also, the previous research of the grounding grid behavior via transients is summarized and discussed. Furthermore, many grounding grid configurations that consist of one, four, and sixteen meshes are simulated using ATP/EMTP. The developed model of the ground grid is verified via a comparison with a published study.

Overvoltages and overcurrents are counted through many case studies. Also, two injection points are analyzed: at the terminal and the middle of the grid. Many transient responses of voltages and currents at different points of the grounding grid for different configurations are calculated. The peak voltage and current values are compared. It is found that the overvoltages are reduced when the lightning is injected at the middle of the ground grid. Whereas the overcurrents are increased in the same case. Therefore, more detailed studies and analysis are required for the best estimation of ground voltages and currents. Also, overvoltage mitigation techniques must be studied for ensuring safe step and touch voltages.

Acknowledgment

The authors thank all institutes they belong to.

Author Contributions

All authors have participated in (a) conception and design, or analysis and interpretation of the data and (b) drafting the article or revising it critically for important intellectual content.

References

[1] POPOV, M., L. GRCEV, H. K. HOIDALEN, B. GUSTAVSEN, V. TERZIJA. Investigation of the Overvoltage and Fast Transient Phenomena on Transformer Terminals by Taking Into Account the Grounding Effects. *IEEE Transactions on Industry Applications*. 2015, vol. 51, no. 6, pp. 5218-5227. DOI: 10.1109/TIA.2015.2411652.

[2] MCDONALD, J. D.. Electric Power Substations Engineering. *Boca Raton, FL, USA: CRC Press*. 2012.

[3] ANSI / IEEE Std 80-2000. IEEE guide for safety in AC substation grounding. *IEEE Power Eng. Soc., Piscataway, NJ, USA*. 2000.

[4] MITOLO, M.. Of Electrical Distribution Systems With Multiple Grounded Neutrals. *IEEE Transactions on Industry Applications*. 2010, vol. 46, no. 4, pp. 1541-1546. DOI: 10.1109/TIA.2010.2051061.

[5] POPOVIĆ, L. M.. Notice of Retraction: Influence of Metal Installations Surrounding the Feeding Cable Line on the Ground Fault Current Distribution in Supplied Substations. *IEEE Transactions on Power Delivery*. 2008, vol. 23, no. 4, pp. 2583-2590. DOI: 10.1109/TPWRD.2008.923502.

[6] PONS, E., P. COLELLA, R. NAPOLI, R. TOMMASINI. Impact of MV Ground Fault Current Distribution on Global Earthing Systems. *IEEE Transactions on Industry Applications*. 2015, vol. 51, no. 6, pp. 4961-4968. DOI: 10.1109/TIA.2015.2417836.

[7] EL-REFAIE, E. S. M., S. E. ELMASRY, M. K. ABD ELRAHMAN, M. H. ABDO. Achievement of the best design for unequally spaced grounding grids. *Ain Shams Engineering Journal*. 2015, vol. 6, no. 1, pp. 171–179. DOI: 10.1016/j.asej.2014.09.013.

[8] NEDI, F.. A new evolutionary method for designing grounding grids by touch voltage control. *2004 IEEE International Symposium on Industrial Electronics, Ajaccio, France*. 2004, vol. 2, pp. 1501-1505. DOI: 10.1109/ISIE.2004.1572036.

[9] GUPTA, B. R., B. THAPAR. Impulse Impedance of Grounding Grids. *IEEE Transactions on Power Apparatus and Systems*. 1980, vol. PAS-99, no. 6, pp. 2357-2362. DOI: 10.1109/TPAS.1980.319800.

[10] GUPTA, B. R., B. THAPAR. Power System Analysis. *McGraw-Hill International Edition*. 1994.

[11] DELVECCHIO, M. S. L. G., F. NERI. A Genetic Algorithm Method for determining the Maximum Touch Voltage generated by a Grounding System. *Optimization and Inverse Problems in Electromagnetism*. 2003.

[12] Estimating lightning performance of transmission lines. II. Updates to analytical models. *IEEE Transactions on Power Delivery*. 1993, vol. 8, no. 3, pp. 1254-1267. DOI: 10.1109/61.252651.

[13] FRESCHI, F., A. GUERRISI, M. TARTAGLIA, M. MITOLO. Numerical Simulation of Heart-Current Factors and Electrical Models of the Human Body. *IEEE Transactions on Industry Applications*. 2013, vol. 49, no. 5, pp. 2290-2299. DOI: 10.1109/TIA.2013.2261042.

[14] IEEE Guide for Safety in AC Substation Grounding. *IEEE Std 80-2000*. 2000, pp.1-192. DOI: 10.1109/IEEESTD.2000.91902.

[15] DOMMEL, H. W.. EMTP Theory Book. *Bonneville Power Administration, Portland*. 1986.

[16] DATPDRAW version 5.6 Users' Manual. 2009.

[17] IEEE Guide for Measuring Earth Resistivity, Ground Impedance, and Earth Surface Potentials of a Ground System Part 1: Normal Measurements. *IEEE Std 81-1983*. 1983, pp.1-44. DOI: 10.1109/IEEESTD.1983.82378.

[18] EL-DESSOUKY, S. S., M. A. EL- AZIZ, A. KHAMIS. An accurate design of substation grounding system aid expert system methodology. *Conference Record of the 1998 IEEE International Symposium on Electrical Insulation (Cat. No.98CH36239), Arlington, VA, USA*. 1998, vol. 2, pp. 411-414. DOI: 10.1109/ELINSL.1998.694821.

[19] HUANG, L., X. CHEN, H. YAN. Study of unequally spaced grounding groups. *IEEE Transactions on Power Delivery*. 1995, vol. 10, no. 2, pp. 716-722. DOI: 10.1109/61.400860.

[20] SUN, W., et al. Optimal design analysis of grounding grids for substations built in nonuniform soil. *PowerCon 2000. 2000 International Conference on Power System Technology. Proceedings (Cat. No.00EX409), Perth, WA, Australia*. 2000, vol. 3, pp. 1455-1460. DOI: 10.1109/ICPST.2000.898183.

[21] PHITHAKWONG, B., et al. New techniques the computer-aided design for substation grounding. *2000 IEEE Power Engineering Society Winter Meeting. Conference Proceedings (Cat. No.00CH37077), Singapore*. 2000, vol. 3, pp. 2011-2015. DOI: 10.1109/PESW.2000.847662.

[22] OTERO, A. F., J. CIDRAS, C. GARRIDO. Genetic algorithm based method for grounding grid design. *1998 IEEE International Conference on Evolutionary Computation Proceedings. IEEE World Congress on Computational Intelligence (Cat. No.98TH8360), Anchorage, AK, USA*. 1998, pp. 120-123. DOI: 10.1109/ICEC.1998.699391.

[23] COSTA, M. C., M. L. P. FILHO, Y. MARECHAL, J.-L. COULOMB, J. R. CARDOSO. Optimization of grounding grids by response surfaces and genetic algorithms. *IEEE Transactions on Magnetics*. 2003, vol. 39, no. 3, pp. 1301-1304. DOI: 10.1109/TMAG.2003.810199.

[24] SAEID, G. F., et al. Investigation and Optimization of Grounding Grid Based on Lightning Response by Using ATP-EMTP and Genetic Algorithm. *Complexity*. 2018. DOI: 10.1155/2018/8261413.

[25] FARKOUSH, S. G., et al. Reducing the Effect of Lightning on Step and Touch Voltages in a Grounding Grid Using a Nature-Inspired Genetic Algorithm With ATP-EMTP. *IEEE Access*. 2019, vol. 7, pp. 81903-81910. DOI: 10.1109/ACCESS.2019.2923656.

[26] CELLI, G., E. GHIANI, F. PILO. Behaviour of grounding systems: a quasi-static EMTP model and its validation. *2010 30th International Conference on Lightning Protection (ICLP), Cagliari, Italy*. 2010, pp. 1-6. DOI: 10.1109/ICLP.2010.7845954.

[27] LONG, X., M. DONG, W. XU, Y. W. LI. Online Monitoring of Substation Grounding Grid Conditions Using Touch and Step Voltage Sensors. *IEEE Transactions on Smart Grid*. 2012, vol. 3, no. 2, pp. 761-769. DOI: 10.1109/TSG.2011.2175456.

[28] TAHER, A., A. SAID, T. ELIYAN, A. HAFEZ. Analysis and Mitigation of Ground Grid Lightning Potential Rise. *Transactions on Electrical and Electronic Materials*. 2020, vol. 21, pp. 305–314. DOI: 10.1007/s42341-020-00186-z.

[29] SUPANUS, K., W. THANSIPHRASERTH, N. RUGTHAICHAROENCHEEP, A. PHAYOMHOM. External grounding design to reduce effects of lightning damage in distribution system. *7th IET International Conference on Power Electronics, Machines and Drives (PEMD 2014), Manchester, UK*. 2014, pp. 1-6. DOI: 10.1049/cp.2014.0415.

[30] GERI A., S. F. VISACRO. Grounding systems under surge conditions: comparison between a field model and a circuit model. *Proc. of 26th ICLP, Krakow, Poland*. 2002, pp. 411-417.

[31] ANDRADE, A. F., et al. Modeling Grounding Systems Response to Current Impulses Considering Nonlinear Effects. *IEEE Transactions on Power Delivery*. 2021, vol. 36, no. 6, pp. 3858-3866. DOI: 10.1109/TPWRD.2021.3049908.

[32] GOUDA, O. E., G. M. AMER, T. M. EL-SAIED. Factors Affecting Transient Response of Ground Grid Systems. *MEPCON Conference*. 1998.